Available online at www.sciencedirect.com
ScienceDirect
Journal of Power Sources 174 (2007) 519–523
JOURNAL OF POWER SOURCES
www.elsevier.com/locate/jpowsour

Short communication

Comparative analysis of the changes in local Ni/Mn environment in lithium–nickel–manganese oxides with layered and spinel structure during electrochemical extraction and reinsertion of lithium

E. Zhecheva [a,*], R. Stoyanova [a], R. Alcántara [b], P. Lavela [b], J.L. Tirado [b]

[a] *Institute of General and Inorganic Chemistry, Bulgarian Academy of Sciences, 1113 Sofia, Bulgaria*
[b] *Laboratorio de Quimica Inorgánica, Facultad de Ciencias, Universidad de Córdoba, 14071 Córdoba, Spain*

Available online 28 June 2007

Abstract

Electron paramagnetic resonance spectroscopy was used to analyse the changes in local Ni, Mn environment in layered $LiNi_{1/2}Mn_{1/2}O_2$ and spinel $LiNi_{1/2}Mn_{3/2}O_4$ after electrochemical extraction and reinsertion of lithium. For layered $LiNi_{1/2}Mn_{1/2}O_2$, the EPR signal from Mn^{4+} is only detected, while residual antiferromagnetic correlations between Ni^{2+} and Mn^{4+} ions gives rise to strong resonance absorption for $LiNi_{1/2}Mn_{3/2}O_4$ spinel. The first charge process of layered $LiNi_{1/2}Mn_{1/2}O_2$ leads to oxidation of Ni^{2+} ions located both in the transition metal sites and in the Li sites. The reverse process of reduction of these nickel ions was suggested to proceed between 4.4–3.0 V and 2.5–1.4 V, respectively. Lithium extraction from $LiNi_{1/2}Mn_{3/2}O_4$ spinel leads to oxidation of paramagnetic Ni^{2+} to diamagnetic Ni^{4+} without significant changes in the local environment of Mn^{4+}. For both fully delithiated compositions, $Li_{1-x}Ni_{1/2}Mn_{1/2}O_2$ and $Li_{1-x}Ni_{1/2}Mn_{3/2}O_4$, an EPR spectrum from localized Mn^{4+} ions is observed, indicating an exhaustion of paramagnetic Ni^{2+} ions in the vicinity of Mn^{4+} ions. Furthermore, it has been found that the Mn^{4+} environment including paramagnetic Mn^{4+} and Ni^{2+} neighbours is restored after the first cycle of charge/discharge.

Keywords: Electrode materials; EPR spectroscopy; Local structural characterization; Lithium-ion batteries

1. Introduction

Lithium–nickel–manganese oxides have been considered as alternative to $LiCoO_2$-based electrode materials for lithium-ion batteries [1–3]. There are two compositions of both research and technological interest: $LiNi_{1/2}Mn_{1/2}O_2$ with layered crystal structure and $LiNi_{1/2}Mn_{3/2}O_4$ with spinel crystal structure. While the layered composition delivers a higher capacity in a lower potential range (about 4 V [1,4–6]), the reversible lithium extraction/insertion from/in the spinel proceeds at a higher potential (4.7 V [2,7–9]). The charge compensation for both compositions is achieved by Ni^{2+} and Mn^{4+} ions. The electrochemical reaction takes place by oxidation/reduction of Ni^{2+} to Ni^{4+}, Mn^{4+} remains inactive [10–14]. In order to improve their electrochemical performance, a more detailed study of the relationship between the local effect in solids and their intercalation properties is to be carried out.

The aim of this contribution is to compare the changes in the local Ni/Mn environment in layered $LiNi_{1/2}Mn_{1/2}O_2$ and spinel $LiNi_{1/2}Mn_{3/2}O_4$ during electrochemical extraction and reinsertion of lithium. A suitable spectroscopic method for monitoring of the Mn/Ni environment in oxides is the electron paramagnetic resonance (EPR). Irrespective of the fact that more than one paramagnetic ions appear in both compositions (Ni^{2+} with $S = 1$ and Mn^{4+} with $S = 3/2$) this method has been already applied for the study of their cationic distribution [15–17]. Here we extend this study in respect of reversible Li deintercalation/intercalation.

2. Experimental

The layered $LiNi_{1/2}Mn_{1/2}O_2$ and spinel $LiNi_{1/2}Mn_{3/2}O_4$ compositions were prepared by solid state reaction. The synthesis procedure is described elsewhere [15–17]. The $LiNi_{1/2}Mn_{1/2}O_2$ composition exhibits layered crystal structure (R-3m space group) with the following structural parameters: $a = 2.8844$ Å, $c = 14.2999$ Å and $z = 0.2582$. Structural refinement of the XRD patterns shows that 0.099 Ni and 0.901 Li reside the 3b-site (LiO_2-layers), and 0.099 Li, 0.401 Ni and

* Corresponding author. Tel.: +359 2 9793915; fax: +359 2 8705024.
E-mail address: zhecheva@svr.igic.bas.bg (E. Zhecheva).

0378-7753/$ – see front matter © 2007 Elsevier B.V. All rights reserved.
doi:10.1016/j.jpowsour.2007.06.127

0.50 Mn are in 3a position (transition metal layers). In cubic spinel notation, the unit cell parameter of $LiNi_{1/2}Mn_{3/2}O_4$ is $a = 8.1530$ Å. A structural difference for the two compositions comes also from their cationic distribution in the transition metal positions. For $LiNi_{1/2}Mn_{3/2}O_4$ spinel, 1:3 Ni:Mn cationic order has been established [15]: each Ni^{2+} is surrounded by 6 Mn^{4+} ions and each Mn^{4+} is in the environment of 4 Mn^{4+} and 2 Ni^{2+} ions. For layered $LiNi_{1/2}Mn_{1/2}O_2$, a short-range Ni, Mn cationic order has been observed [16]: a fraction of Mn^{4+} ions are in mixed Li, Ni, Mn environment resembling that of "α,β"-cationic distribution in Li_2MnO_3, while the rest of Mn^{4+} ions are in Ni, Mn environment with statistical distribution.

The EPR spectra were recorded as a first derivative of the absorption signal of an ERS-220/Q (ex-GDR) spectrometer within the temperature range of 90–400 K. The *g* factors were determined with respect to a Mn^{2+}/ZnS standard. The signal intensity was established by double integration of the experimental EPR spectrum. The analytical amount of Mn^{4+} was determined relative to Li_2MnO_3 standard. To obtain the ex situ EPR spectra of the electrodes, the electrochemical process was interrupted at selected charge levels and then, after a relaxation period, the electrochemical cells were dismounted in an Ar-containing dry-box and the electrodes were recuperated. The lithium content of the charged/discharged samples was calculated assuming that no current was consumed in side reactions. This means that the charge/discharge level is overestimated and the lithium contents correspond to nominal compositions.

The electrochemical oxidation/reduction of oxides was carried out by using two-electrode Swagelok™ cells of the type $Li|LiPF_6(EC:DEC)|Li_xM_yO_2$. The positive electrode, having about 4 mg cm^{-2} of active material supported onto an aluminum foil (Goodfellow), was prepared as 9 mm diameter disk by drying at 120 °C into vacuum and pressing then a mixture of 80% of the active oxide, 5% of PVDF binder, and 15% of carbon (50% weight mixture of graphite and carbon black) previously dispersed in 1-methyl-2-pyrrolidone. Lithium electrodes consisted of a clean 9 mm diameter lithium metal disk. The commercial (Merck LP40) electrolyte solution was 1 M $LiPF_6$ in a 1:1 (w/w) mixture of ethylene carbonate (EC) and diethyl carbonate (DEC) that was supported by porous glass-paper discs Whatman™ as separators. The electrochemical reactions were carried out by using a multichannel MacPile II system in potentiostatic mode at 10 mV/0.1 h of scan rate. The cells were mounted in a dry box under Ar atmosphere.

3. Results and discussion

Mass-normalized intensity versus voltage curves of layered-type $LiNi_{0.5}Mn_{0.5}O_2$ electrodes display a broadened signal located between 3.7 and 4.6 V in the charge process, and between 3.0 and 4.4 V in the discharge process (Fig. 1). In contrast, spinel-type $LiNi_{0.5}Mn_{1.5}O_4$ electrodes show the oxidation and subsequent reduction in poorly resolved double peaks in the 4.5–5.0 V region. According to previous studies [10–14], the signals are ascribed to the Ni^{4+}/Ni^{2+} redox couple and lithium ordering processes.

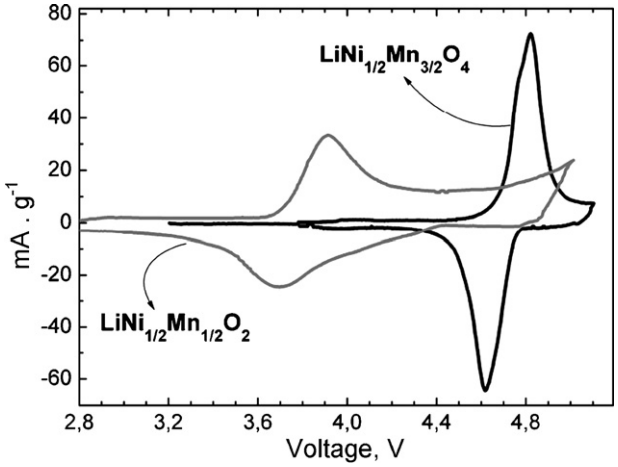

Fig. 1. Potentiostatic curves corresponding to first charge/discharge cycle of layered $LiNi_{1/2}Mn_{1/2}O_2$ and $LiNi_{1/2}Mn_{3/2}O_4$ spinel in lithium cells.

Fig. 2 compares the EPR spectra of pristine layered and spinel compositions ($LiNi_{1/2}Mn_{1/2}O_2$ and $LiNi_{1/2}Mn_{3/2}O_4$). Above 140 K, the EPR spectra of both compositions consist of a single Lorentzian line. Below 140 K, the EPR signal from $LiNi_{1/2}Mn_{3/2}O_4$ spinel disappears, while the EPR response from layered $LiNi_{1/2}Mn_{1/2}O_2$ is still visible. At this temperature, it has been found that $LiNi_{1/2}Mn_{3/2}O_4$ spinel undergoes a ferromagnetic transition, while no long magnetic range order was observed for layered $LiNi_{1/2}Mn_{1/2}O_2$ up to 5 K [18,19]. For both compositions, the effective g-factor decreases on cooling from 413 K (Fig. 3). There is a line narrowing from 413 to 143 K for $LiNi_{1/2}Mn_{3/2}O_4$ spinel, while a slight line broadening is observed for layered $LiNi_{1/2}Mn_{1/2}O_2$. Based on previous EPR studies [15–17], the EPR response from $LiNi_{1/2}Mn_{3/2}O_4$ spinel is due to the residual antiferromagnetic correlations between Ni^{2+} and Mn^{4+} ions, while only Mn^{4+} ions gives rise to the EPR profile of layered $LiNi_{1/2}Mn_{1/2}O_2$.

Fully delithiated layered and spinel compositions display completely different EPR spectra (Fig. 2). For layered $Li_{\delta\to 0}Ni_{1/2}Mn_{1/2}O_2$ with nominal lithium content close to 0, only one broad signal is observed. For $Li_{\delta\to 0}Ni_{1/2}Mn_{3/2}O_4$ spinel, two signal can be resolved: at 293 K, a narrow Lorentzian dominates the EPR spectrum, whereas a broader Lorentzian is better visible on cooling. The intensity of the broader signal is about 10 times higher than that of the narrower. The effective *g*-factors for both fully delithiated oxides remain the same in the temperature range of 100–300 K in contrast to that of the pristine compositions (Fig. 3): the *g*-value for layered $Li_{\delta\to 0}Ni_{1/2}Mn_{1/2}O_2$ tends to 1.99, while for $Li_{\delta\to 0}Ni_{1/2}Mn_{3/2}O_4$ spinel $g = 2.002$ and 2.09 for the narrower and the broader signals, respectively. These results show that the EPR signals for both completely delithiated compositions come from localized Mn^{4+} ions which are in the environment of allied Mn^{4+} and diamagnetic ions (such as Ni^{4+} and Li^+). This is related with the oxidation of paramagnetic Ni^{2+} ions in the vicinity of Mn^{4+} into diamagnetic Ni^{4+} ions after complete removal of Li.

For fully delithiated spinel, $Li_{\delta\to 0}Ni_{1/2}Mn_{3/2}O_4$ the observation of two EPR signals is related with two-phase mechanism

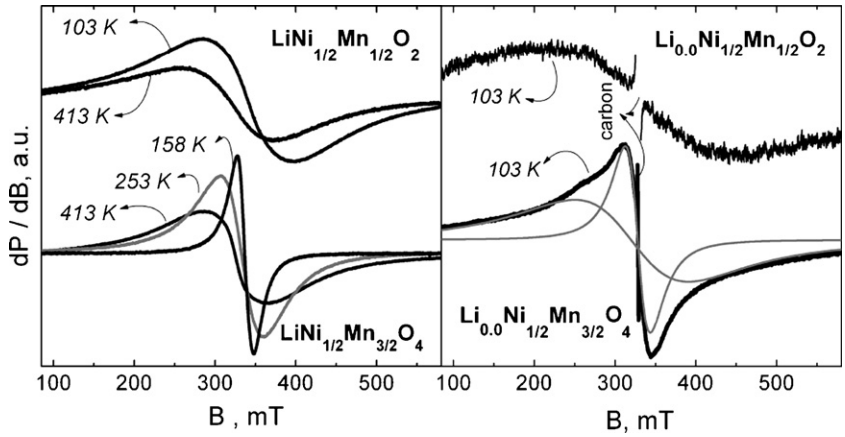

Fig. 2. EPR spectra of pristine layered $LiNi_{1/2}Mn_{1/2}O_2$ and $LiNi_{1/2}Mn_{3/2}O_4$ spinel and electrodes after first charge up to 5.1 V (with nominal compositions corresponding to $Li_{\delta\to 0}Ni_{1/2}Mn_{1/2}O_2$ and $Li_{\delta\to 0}Ni_{1/2}Mn_{3/2}O_4$, respectively). Two simulated signals detected at $Li_{\delta\to 0}Ni_{1/2}Mn_{3/2}O_4$ are indicated. The signal from carbon mixture is also shown.

of lithium extraction. This result can be understood if we take into account the dependence of the magnetic Mn^{4+}–Mn^{4+} interactions on the distance. The magnetic behaviour of the manganese spinels is determined from the competition between direct Mn^{4+}–Mn^{4+} antiferromagnetic and 90° superexchange Mn^{4+}–O^{2-}–Mn^{4+} ferromagnetic interactions [20,21]. Thus, it has been shown that superexchange ferromagnetic interactions dominates for Mn^{4+}-containing spinels where the Mn–Mn contact is between 2.867(4) and 2.923(4) Å (such as $LiMg_{1/2}Mn_{3/2}O_4$ [19]), while an antiferromagnetic character is reported for spinels with $r_{Mn-Mn} = 2.84$ and 2.85 Å (such as λ-MnO_2 and $LiCoMnO_4$, respectively [22,23]). $Li[Li_{1/3}Mn_{5/3}]O_4$ composition having $r_{Mn-Mn} = 2.87$ Å is near the crossover between the ferromagnetic and antiferromagnetic transition [21]. Accordingly, this composition displays a broader EPR signal as compared to that of $LiMg_{1/2}Mn_{3/2}O_4$ and $LiCoMnO_4$: the line width is about 100 mT, 44 mT and 22 mT for $Li[Li_{1/3}Mn_{5/3}]O_4$, $LiMg_{1/2}Mn_{3/2}O_4$ and $LiCoMnO_4$, respectively [24]. The temperature variation of the EPR line width for Mn^{4+}-containing spinels is a result from the development of ferro- or antiferromagnetic interactions. The EPR line width decreases on cooling for ferromagnetically coupled Mn^{4+}, while for antiferromagnetically coupled Mn^{4+} there is an increase of the EPR line width. For fully delithiated $Li_{0.0}Ni_{1/2}Mn_{3/2}O_4$ spinel, the line width for the narrow signal increases on cooling, while the broader signal is slightly narrowed below 173 K (Fig. 3). Based on this comparison, one may suggest that the narrow signal corresponds to an antiferromagnetic spinel phase with a contracted lattice constant ($r_{Mn-Mn} \approx 2.85$ Å or $a \sim 8.05$ Å), whereas a spinel phase with an expanded lattice constant ($r_{Mn-Mn} \approx 2.87$ or $a \sim 8.13$ Å) is responsible for the appearance of the broader signal. This result is consistent with the ex situ XRD data on the changes of the lattice constant of $LiNi_{1/2}Mn_{3/2}O_4$ during electrochemical extraction of Li [8,9,25,26].

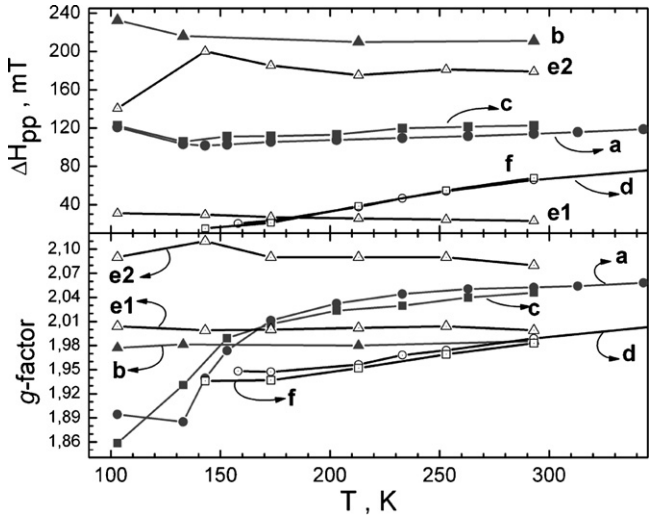

Fig. 3. Temperature dependence of the EPR line width, ΔH_{pp}, and g-factor for pristine $LiNi_{1/2}Mn_{1/2}O_2$ (a) and $LiNi_{1/2}Mn_{1/2}O_2$ electrodes obtained: after first charge to 5.1 V (b); after first charge/discharge to 2.5 V (c). Temperature dependence of ΔH_{pp}, and g-factor for pristine $LiNi_{1/2}Mn_{3/2}O_4$ spinel (d) and $LiNi_{1/2}Mn_{3/2}O_4$ electrodes obtained: after first charge to 5.1 V (e1 and e2); after first charge/discharge to 3.5 V (f).

For partially delithiated spinel, $Li_xNi_{1/2}Mn_{3/2}O_4$, the Ni^{2+}–Mn^{4+} spin system remains unchanged. The EPR intensity is reduced following the changes in the Li amount: from $I = 1.0$ to 0.67 and 0.17 for initial and after 30% and 70% of extracted Li, respectively. This result implies that the electrochemical extraction of Li from $Li_{1.0}Ni_{1/2}Mn_{3/2}O_4$ spinel can be considered as a two-phase reaction including the initial composition and a new phase, which is EPR undetectable. In addition, it is worth comparing the EPR behaviour of $LiNi_{1/2}Mn_{3/2}O_4$ during Li extraction with the ^{6}Li NMR experiments for charged $LiNi_{1/2}Mn_{3/2}O_4$ electrodes [27]. Up to 90% of extraction of Li, NMR spectroscopy shows that charging process involves the Li removal without changes in the Li local environment [27]. On the other hand, it appears that both local EPR and NMR techniques give complementary data to the ex situ XRD experiments [8,9,26].

For partially delithiated layered $Li_xNi_{1/2}Mn_{1/2}O_2$, the Lorentzian signal is extremely broadened. In addition, a new signal grows in intensity at 143 K (Fig. 4). The effective g-factor and the line shape undergo dramatic changes in a narrow temper-

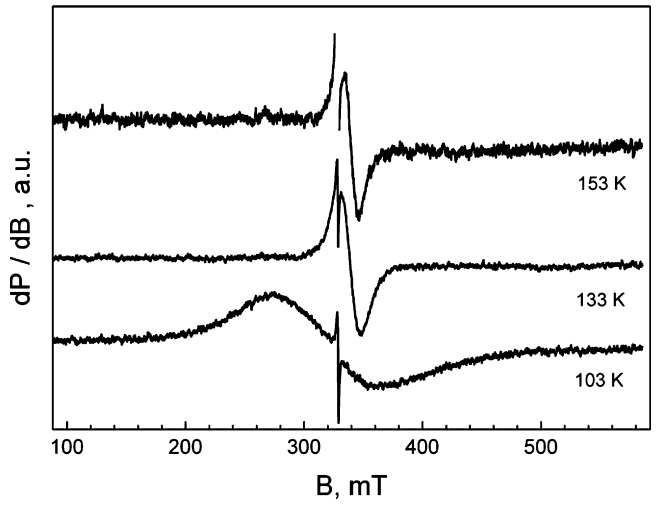

Fig. 4. EPR spectra of the $Li_xNi_{1/2}Mn_{1/2}O_2$ electrode obtained after first charge to 4.5 V (with composition corresponding to $Li_{0.52}Ni_{1/2}Mn_{1/2}O_2$).

ature range: going from 130 to 100 K, the resonance absorption is shifted to lower magnetic fields. Looking for the origin of this signal, it is worth mentioning that after 67% of extracted Li a small fraction of nickel ions in tetrahedral sites have been detected [28]. However, the EPR parameters of the new signal are not consistent with that for Ni^{2+} or Ni^{3+} in tetrahedral coordination. The origin of this signal can be explained having in mind that about 10% of Ni^{2+} resides the Li-sites. An EPR signal with the same parameters has been detected for non-stoichiometric $Li_{1-x}Ni_{1+x}O_2$ with $x < 0.33$, which also contain Ni^{2+} in the Li-sites [29]. The Ni^{2+} and Ni^{3+} located in two adjacent layers are coupled by strong 180° antiferromagnetic interactions. The development of 180° Ni^{2+}–O–Ni^{3+} magnetic coupling between the layers proceeds in addition to the 90° Ni^{3+}–O–Ni^{3+} coupling within the layers. The 180° exchange interactions are stronger than the 90° ones, as a result of which the EPR spectrum changes from localized spin states to magnetically correlated spins at a temperature lower than 210 K [29]. The close EPR parameters observed for partially delithiated $Li_xNi_{0.5}Mn_{0.5}O_2$ and non-stoichiometric $Li_{1-x}Ni_{1+x}O_2$ permit assigning the EPR signal of the former oxide to 180° coupled Ni^{2+}–Ni^{3+} ions occupying both Li- and Ni/Mn-sites.

The signal due to 180° coupled Ni^{2+}–Ni^{3+} ions is observed for partially delithiated layered oxides only, $Li_xNi_{1/2}Mn_{1/2}O_2$. The appearance of the EPR signal in partially delithiated oxides indirectly indicates that Ni^{2+} ions are oxidized via Ni^{3+} ions in the transition metal layers. By increasing the extent of Li extraction, the disappearance of this signal reveals a generation of Ni^{4+} ions in the transition metal layers as oxidation products. In addition, the oxidation of Ni^{2+} in the Li-site cannot be rejected. As a comparison, it is worth mentioning that Ni^{2+} ions in the Li-site are electrochemically inactive for layered non-stoichiometric $Li_{1-x}Ni_{1+x}O_2$ [30].

For layered $LiNi_{1/2}Mn_{1/2}O_2$, the electrochemical activity of Ni^{2+} in the Li-site was demonstrated by electrochemical test in a more extended potential range (Fig. 5). Keeping the lower voltage limit at 2.5 V, the upper voltage limit is decreased from 5.0 to 4.8 V. After 18 cycles between 4.8 and 2.5 V, there is a gradual loss in initial capacity: from 160 to 90 mAh g. By extending the lower voltage limit from 2.5 to 1.45 V, the reversible capacity immediately increases to 160 mAh g. In the discharge curve, a redox reaction between 2.5 and 2.0 V is clearly resolved, while only one oxidation reaction is visible above 4.2 V on the charge curve (Fig. 5A). Fig. 5B gives the EPR spectrum of the corresponding sample obtained after 18 cycles between 2.5–4.8 V and subsequent 19 cycles between 1.45–4.8 V and stopped at 1.45 V. At a lower registration temperature, two overlapping signals can be resolved. The first signal corresponds to the main signal due to Mn^{4+} ions in $LiNi_{1/2}Mn_{1/2}O_2$. The second signal bears characteristics of the signal due to 180° coupled Ni^{2+}–Ni^{3+} ions. It is important to note that this signal is not registered in the case when oxides are cycled between 4.6 and 2.7 V. This means that Ni^{2+} ions in the Li-sites are generated and detected by EPR in the oxides cycled in the lower potential range. The reappearance of Ni^{2+} in the Li-sites of oxides cycled at 4.8–1.45 V can be tentatively associated with the redox reaction occurring between 2.0 and 2.5 V. It is important to note that, according to Thackeray et

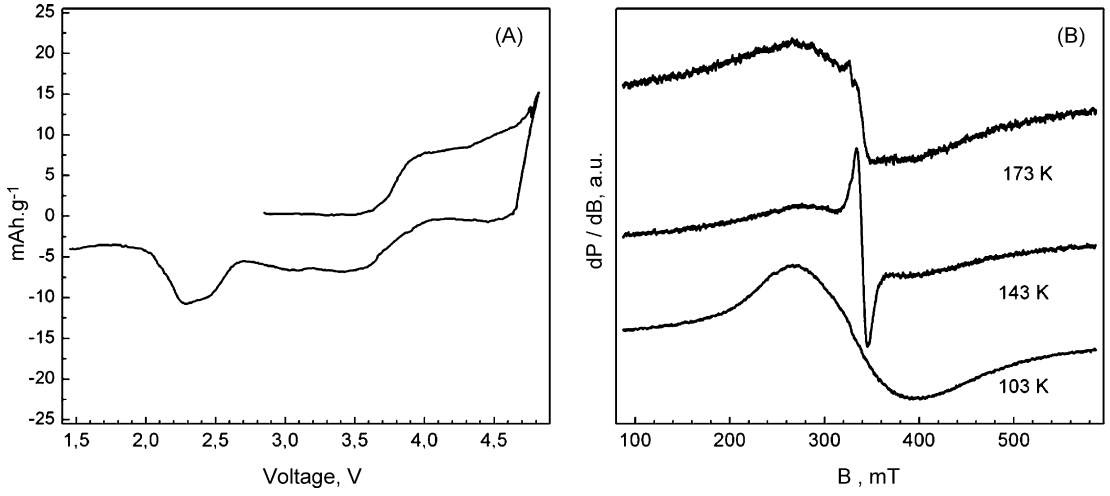

Fig. 5. (A) Mass-normalized intensity vs. voltage curves of layered $LiNi_{1/2}Mn_{1/2}O_2$ after 18 cycles at 4.8–2.5 V. (B) EPR spectra of the $LiNi_{1/2}Mn_{1/2}O_2$ electrode obtained after 18 cycles at 4.8–2.5 V and subsequent 11 cycles at 4.8–1.45 V.

al. [31], up to 1.4 V Mn remains tetravalent, while between 2.5 and 1.4 V there was reduction of residual Ni^{3+} in the electrode to Ni^{2+}.

For both layered and spinel compositions, Li reinsertion causes a recovering of the EPR spectra in terms of the temperature dependence of the EPR line width and effective *g*-factor (Fig. 3). This means that the Mn^{4+} environment in respect of paramagnetic Mn^{4+} and Ni^{2+} neighbors is restored after the first cycle: 2.5–5.1 V for layered $Li_{1.0}Ni_{1/2}Mn_{1/2}O_2$ and 3.2–5.1 V for $Li_{1.0}Ni_{1/2}Mn_{3/2}O_4$ spinel.

4. Conclusions

Lithium extraction from $Li_{1.0}Ni_{1/2}Mn_{3/2}O_4$ spinel can be regarded as a two-phase reaction including the initial composition and a new phase, which is EPR undetectable. Lithium extraction from layered $LiNi_{1/2}Mn_{1/2}O_2$ up to 5.1 V proceeds by the oxidation of Ni^{2+} ions located both in the transition metal layers and the lithium layers, while the reverse process of reduction takes place between 4.4–3.0 V and 2.5–1.4 V, respectively.

Lithium reinsertion in layered $LiNi_{1/2}Mn_{1/2}O_2$ and $LiNi_{1/2}Mn_{3/2}O_4$ spinel shows a good recovering of the initial properties making evident the notorious reversibility of these electrode materials.

Acknowledgments

Authors are indebted to the National Science Fund of Bulgaria (Contract no. Ch1304/2003) for partial financial support. Authors are grateful to EC for financial support within the Centre of Competence MISSION (Specific Support Action, EC-INCO-CT-2005-016414) and CICYT (MAT2005-000374).

References

[1] M.E. Spahr, P. Novák, B. Schnyder, O. Haas, R. Nesper, J. Electrochem. Soc. 145 (1998) 1113.
[2] Q. Zhong, A. Bonakdarpour, M. Zhang, Y. Gao, J.R. Dahn, J. Electrochem. Soc. 144 (1997) 205.
[3] M.S. Whittingham, Chem. Rev. 104 (2004) 4271.
[4] T. Ohzuku, Y. Makimura, Chem. Lett. (2001) 744.
[5] Z. Lu, D.D. MacNeil, J.R. Dahn, Electrochem. Solid-State Lett. 4 (2001) A191.
[6] J.-S. Kim, G.S. Johnson, M.M. Thackeray, Electrochem. Commun. 4 (2002) 205.
[7] K. Ariyoshi, S. Yamamoto, T. Ohzuku, J. Power Sources 119–121 (2003) 959.
[8] R. Alcántara, M. Jaraba, P. Lavela, J.L. Tirado, Electrochim. Acta 47 (2002) 1829.
[9] S.-T. Myung, S. Komaba, N. Kumagai, H. Yashiro, H.-T. Chung, T.-H. Cho, Electrochim. Acta 47 (2002) 2543.
[10] Z. Lu, L.Y. Beaulieu, R.A. Donaberger, C.L. Thomas, J.R. Dahn, J. Electrochem. Soc. 149 (2002) A778.
[11] J. Reed, G. Ceder, Electrochem. Solid-State Lett. 5 (2002) A145.
[12] M. Saiful Islam, R. Andrew Davis, J.D. Gale, Chem. Mater. 15 (2003) 4280.
[13] K. Amine, H. Tukamoto, H. Yasuda, Y. Fujita, J. Electrochem. Soc. 143 (1996) 1607.
[14] M. Okada, Y.-S. Lee, M. Yoshio, J. Power Sources 90 (2000) 196.
[15] R. Alcántara, M. Jaraba, P. Lavela, J.L. Tirado, E. Zhecheva, R. Stoyanova, Chem. Mater. 16 (2004) 1573.
[16] R. Stoyanova, E. Zhecheva, S. Vassilev, J. Solid State Chem. 179 (2006) 378.
[17] R. Stoyanova, E. Zhecheva, R. Alcántara, J.L. Tirado, J. Mater. Chem. 16 (2006) 359.
[18] S.-H. Kang, J. Kim, M.E. Stoll, D. Abraham, Y.K. Sun, K. Amine, J. Power Sources 112 (2002) 41.
[19] W. Branford, M.A. Green, D.A. Neumann, Chem. Mater. 14 (2002) 1649.
[20] G. Blasse, J. Phys. Chem. Solids 27 (1966) 383.
[21] C. Masquelier, M. Tabuchi, K. Ado, R. Kanno, Y. Kobayashi, Y. Maki, O. Nakamura, J.B. Goodenough, J. Solid State Chem. 123 (1996) 255.
[22] J.E. Greedan, N.P. Raju, A.S. Wills, C. Morin, S.M. Shaw, J.N. Reimers, Chem. Mater. 10 (1998) 3058.
[23] B. Gee, C.R. Horne, E.J. Cairns, J. Reimer, J. Phys. Chem. B 102 (1998) 10142.
[24] R. Stoyanova, E. Zhecheva, Solid State Commun. 135 (2005) 405.
[25] K. Ariyoshi, Y. Iwakoshi, N. Nakayama, T. Ohzuku, J. Electrochem. Soc. 151 (2004) A296.
[26] M. Mohamedi, M. Makino, K. Dokko, T. Itoh, I. Uchida, Electrochim. Acta 48 (2002) 79.
[27] Y.-J. Lee, C. Eng, C.P. Grey, J. Electrochem. Soc. 148 (2001) A249.
[28] Y. Arachi, H. Kobayashi, S. Emura, Y. Nakata, M. Tanaka, T. Asai, H. Sakaebe, K. Tatsumi, H. Kageyama, Solid State Ionics 176 (2005) 895.
[29] R. Stoyanova, E. Zhecheva, C. Friebel, Solid State Ionics 73 (1994) 1.
[30] C. Delmas, M. Menetrier, L. Croguennec, I. Saadoune, A. Rougier, C. Poillerie, G. Prado, M. Grüne, L. Fournes, Electrochim. Acta 145 (1999) 243.
[31] C.S. Johnson, A.J. Kahaian, J.S. Kim, A.J. Kropf, J.T. Vaughey, M.M. Thackeray, Electrochem. Commun. 4 (2002) 492.